strain
An International Journal for Experimental Mechanics

An Analytical Model Based on Strain Localisation for the Study of Size-Scale and Slenderness Effects in Uniaxial Compression Tests

A. Carpinteri, M. Corrado and M. Paggi

Politecnico di Torino, Department of Structural and Geotechnical Engineering, C.so Duca degli Abruzzi 24, 10129 Torino, Italy

ABSTRACT: In this paper, an analytical model based on the concept of strain localisation is proposed for the analysis and prediction of the response of quasi-brittle materials in uniaxial compression tests, such as mortar, plain concrete with different compression strengths, as well as fibre-reinforced concrete. The proposed approach, referred to as *Overlapping Crack Model*, relies only on a pair of material constitutive laws, in close analogy with the *Cohesive Crack Model*: a stress–strain relationship describing the pre-peak behaviour of the material and a stress–interpenetration relationship for the description of the post-peak response. In the paper it will be shown how the stress–interpenetration relationship can be deduced from experimental data and how it depends on the compression strength and on the crushing energy of the tested materials. A wide comparison between the stress–displacement curves predicted by the proposed model and those experimentally found in the literature will show the effectiveness of the present approach to capture both stable softening or sharp snap-back post-peak branches by varying the slenderness or the size-scale of the tested samples.

KEY WORDS: *compression, concrete-like materials, crushing energy, size effects, strain localisation*

Introduction

The compression behaviour of concrete, and in particular the ultimate strength and the post-peak branch, have an important role in the design of concrete and concrete-based structures. Structural design, in fact, is usually conducted by comparing an action with a resistance evaluated on the basis of the ultimate strength. On the other hand, the post-peak behaviour is fundamental for a correct evaluation of the ductility, e.g. the case of the ultimate axial deformation of columns or the rotational capacity of reinforced concrete beams. In this context, size-scale effects play an important role, because of the fact that the characteristic parameters of concrete are measured on specimens at a laboratory scale that is far from the dimension of a real structure.

The correct evaluation of the constitutive parameters is also complicated by many other testing aspects. The original insights provided by Kotsovos [1] and van Mier [2], and further studied in depth by the Round Robin programme carried out by the RILEM Technical Committee 148-SSC [3], put into evidence that the strength of concrete highly depends on friction between concrete and the loading platens, as well as on the slenderness of the specimen (see [4] for a detailed review of the contributions in the literature on this matter). With decreasing slenderness, an increase of specimen strength is measured when rigid steel loading platens are used. On the contrary, when friction-reducing measures are used, for example by inserting a teflon sheet between the steel-loading platen and the concrete specimen, the compression strength measured on prisms or cylinders becomes almost independent of the slenderness ratio, l/h [4, 5]. Moreover, the effect of friction disappears when the specimen slenderness is higher than 2.5. All the experiments of the aforementioned Round Robin revealed also that, in the softening regime, ductility (in terms of stress and strain) is a decreasing function of the slenderness. Furthermore, a close observation of the stress versus post-peak deformation curves showed that a strong localisation of deformations occurs in the softening regime, independently of the loading system, confirming again the earlier results by Kotsovos [1] and van Mier [2]. The phenomenon of strain localisation in compression, evidenced in many other experimental programmes on concrete and rocks [6–10], suggests that, in the softening regime, energy dissipation takes place over an internal surface rather than within a volume, in close

analogy with the behaviour in tension. These two interconnected phenomena may explain the size-scale effects on ductility. Because of strain localisation, the post-peak branch of the stress–strain curve is no longer a true material property but it becomes dependent on the specimen size and slenderness. Based on these experimental evidences, Hillerborg and coworkers [11, 12] proposed to model failure of concrete in compression (*crushing*) by means of strain localisation over a band thickness proportional to the extension of the compressed zone. In this way, the σ–ε relationships used to describe the softening regime permit to address the issue of size effects, although the thickness over which the localisation occurs becomes a free parameter, usually defined by best-fitting of experimental data [13].

More recently, Palmquist and Jansen [14] have proposed an analytical model based on strain localisation and damage mechanics for the analysis of the post-peak behaviour of quasi-brittle materials in compression. After the achievement of the material compression strength, they consider the sample subdivided into two zones: a bulk zone and a damaged one, being their relative sizes dependent on the post-peak stress level. Both zones are characterised by a pair of stress–strain constitutive laws, whose parameters are determined according to a best-fitting procedure on experimental data. The thickness of the damage zone is assumed to be a linear function of the post-peak stress and varies from the width of the specimen up to a maximum of twice the specimen width. These model assumptions present some drawbacks that limit the predictive capabilities of this approach. In fact, the best-fitting parameters of the post-peak stress–strain relationship determined from different sources diverge significantly, although the materials were similar in terms of compression strength. In addition to the impossibility of relating these constants to the material properties of the tested specimens, this model can only be applied to specimens with height–width ratio (slenderness) higher than 2.

Based on the evidence that the post-peak dissipated energy referred to a unitary surface can be considered as a material property [6, 9] and, consequently, that the post-peak stress–displacement relationship is independent of the specimen size [7, 8], Carpinteri *et al.* [15–17] and Corrado [18] have recently proposed to model the process of concrete crushing taking place in reinforced concrete beams in bending using an approach analogous to the *Cohesive Crack Model* [19–22], which is routinely adopted for modelling the tensile behaviour of concrete. In tension, the localised strain is represented by a fictitious crack opening, while in compression it would be represented by an interpenetration. This new approach, which will be detailed in the sequel for the analysis of uniaxial compression tests, is referred to as *Overlapping Crack Model* [15–18] and assumes a stress–displacement law as a material characteristic for the post-peak behaviour of concrete in compression.

In this paper, we first introduce the mathematical aspects of the *Overlapping Crack Model* for the description of concrete crushing in compression, showing that, in close analogy with the *Cohesive Crack Model* in tension, it is possible to fully describe the mechanical behaviour of quasi-brittle materials in compression using a pair of constitutive laws: a stress–strain relationship for the pre-peak stage and a stress–interpenetration relationship for the post-peak branch. It will be shown that the stress–interpenetration relationship is size-scale and slenderness independent and that can be approximated by a simple equation with only one free parameter to be determined from experimental data. A correlation between this best-fitting parameter and the material properties, such as the compression strength and the crushing energy, will also be derived, allowing the applicability of the proposed model to any other quasi-brittle material. In fact, when the material compression strength and the crushing energy are known (determined from a single specimen with a given size and slenderness or deduced from correlations as in [9]), this best-fitting parameter can be determined according to the proposed correlation and can be used to predict stress–displacement curves for different sizes or slendernesses.

Finally, a wide comparison between analytical and experimental stress–displacement curves for mortar, plain concrete and fibre-reinforced concrete (FRC) will show the effectiveness and the accuracy of the present approach to capture stable softening or sharp snap-back post-peak branches by varying the slenderness or the size-scale of the tested samples.

The Proposed Analytical Model

In structural design, the most frequently adopted constitutive laws for concrete in compression describe the material behaviour in terms of stress and strain (elastic-perfectly plastic, parabolic-perfectly plastic, Sargin's parabola, etc.). This classic approach, which implies that the energy is dissipated within a volume, does not permit to describe the post-peak mechanical behaviour of quasi-brittle materials in compression, which is dominated by a strong strain localisation with the appearance of one or more transversal or inclined shear bands [6–9].

In the present formulation, we use the *Overlapping Crack Model* for the analysis of the post-peak response of quasi-brittle materials in compression. This approach, recently proposed in [15–18] for the analysis of the non-linear behaviour of reinforced concrete beams in bending, is analogous to the well-known *Cohesive Crack Model* used to analyse the behaviour of concrete in tension. The main hypotheses of the model are the following:

1 The constitutive law used for the pre-peak stage is mainly characterised by the elastic modulus of the material. Whereas a simple linear elastic stress–strain relationship is adequate for modelling the behaviour of concrete in tension, here we consider the non-linear relationship provided by the Model Code 90 [23], which is well suited for taking into account the non-linear behaviour of concrete in the ascending branch (see Figure 1A):

$$\frac{\sigma}{\sigma_c} = \frac{\frac{E_{ci}}{E_{c1}}\frac{\varepsilon}{\varepsilon_{c1}} - \left(\frac{\varepsilon}{\varepsilon_{c1}}\right)^2}{1 + \left(\frac{E_{ci}}{E_{c1}} - 2\right)\frac{\varepsilon}{\varepsilon_{c1}}}, \tag{1}$$

where σ_c is the compression strength, σ is the actual value of the compression stress, ε is the compression strain, $\varepsilon_{c1} = -0.0022$, E_{ci} is the tangent modulus and E_{c1} is the secant modulus from the origin up to the peak compression stress, σ_c.

2 The crushing zone is assumed to develop when the maximum compression stress reaches the concrete compression strength. The corresponding process zone is considered to be perpendicular to the principal compression stress. The crushing zone is then represented by a fictitious overlapping, which is mathematically analogous to the fictitious crack in tension. It is important to note that, from the mathematical point of view, the overlapping displacement is a global quantity, and therefore it permits to characterise the structural behaviour without the need of modelling into the details the actual failure mode of the specimen, which may vary from pure crushing to diagonal shear failure, or even to splitting, depending on its size-scale and slenderness [3].

3 The damaged material in the process zone is assumed to be able to transfer a compression stress between the overlapping surfaces. Concerning such stresses, they are assumed to be a decreasing function of the interpenetration, w. In tension, the cohesive stresses tend to zero when a critical crack opening displacement is reached. Under compression, the situation is slightly different and experimental results show that the compression stress does not vanish, but it tends to an asymptotic residual value for overlapping displacements larger than the critical interpenetration $w_{cr} \approx 1$ mm (see Figure 1B). The crushing energy, $\mathcal{G}_C$, defined as the area below the post-peak softening curve of Figure 1B, can be considered as a true material property, because it is not affected by the structural size-scale or slenderness. Dahl and Brincker [6] carried out a series of uniaxial compression tests with the aim of measuring the dissipated energy per unit cross-sectional area. They obtained values of about 50 N mm^{-1} for plain concrete samples and claimed that this dissipated energy becomes independent of the specimen size if the specimen is large enough. The effect of lateral confinement due to friction is also important and affects the crushing energy as shown in [1]. However, the normalised stress versus post-peak displacement curves for a given confinement level are grouped within a narrow band. In the case of lateral confinement because of stirrups, the empirical correlations by Suzuki *et al.* [9] can be used to quantify the increase in crushing energy as compared with the unconfined case. It is worth noting that the crushing energy of unconfined concrete is between two and three orders of magnitude higher than the tensile fracture energy, whereas the critical value for the overlapping displacement, w_{cr}, is one order of magnitude higher than the critical opening displacement in tension (see also the experimental results in [8]).

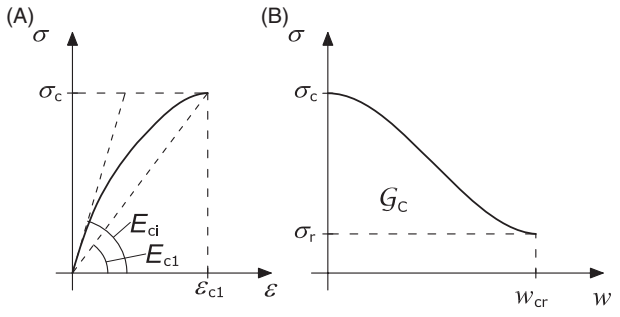

Figure 1: A pair of constitutive laws introduced by the *Overlapping Crack Model* for concrete in compression: (A) a stress–strain law up to the achievement of the concrete compression strength and (B) a stress–displacement relationship describing the effect of strain localisation

From the modelling point of view, the following softening law is herein adopted:

$$\frac{\sigma}{\sigma_c} = \frac{1}{(Aw)^B + 1}, \tag{2}$$

where the parameters A and B can be determined according to a best-fitting procedure of experimental data. Actually, we will show that the

parameter B can be kept equal to 1.67 for all the quasi-brittle materials analysed in the present study and therefore only one free parameter should be tuned on the basis of the experimental results.

Experimentally evaluated stress–interpenetration curves of mortar, plain concrete with different values of compression strength, and FRC available in the literature [8, 24, 25] are shown in Figure 2. The main mechanical parameters of these samples are shown in Table 1. In some cases, the stress–interpenetration diagrams were already available, whereas in other cases the post-peak σ–w relationships are computed from the σ–ε curves in the following way:

1 The relationship between stress and total shortening of the specimen, σ–δ, is obtained by multiplying the strain ε by the length of the specimen, l.

2 The post-peak σ–w relationship is obtained from the σ–δ diagram by subtracting the elastic elongation, caused by the reduction of the applied stress in the post-peak regime, δ_{el}, and the pre-peak plastic deformation, δ_{pl}, as shown in Figure 3. The value of the displacement δ_{el} is given by the following expression:

$$\delta_{el} = \frac{\sigma}{E_{ci}} l \tag{3}$$

where σ is the actual value of the compression stress, E_{ci} is the tangent modulus according to Equation (1), and l is the specimen length.

As can be readily seen from Figure 2, the overlapping crack laws are almost slenderness and size independent. The proposed best-fitting curves are summarised in Figure 2F for each material characterised by a given

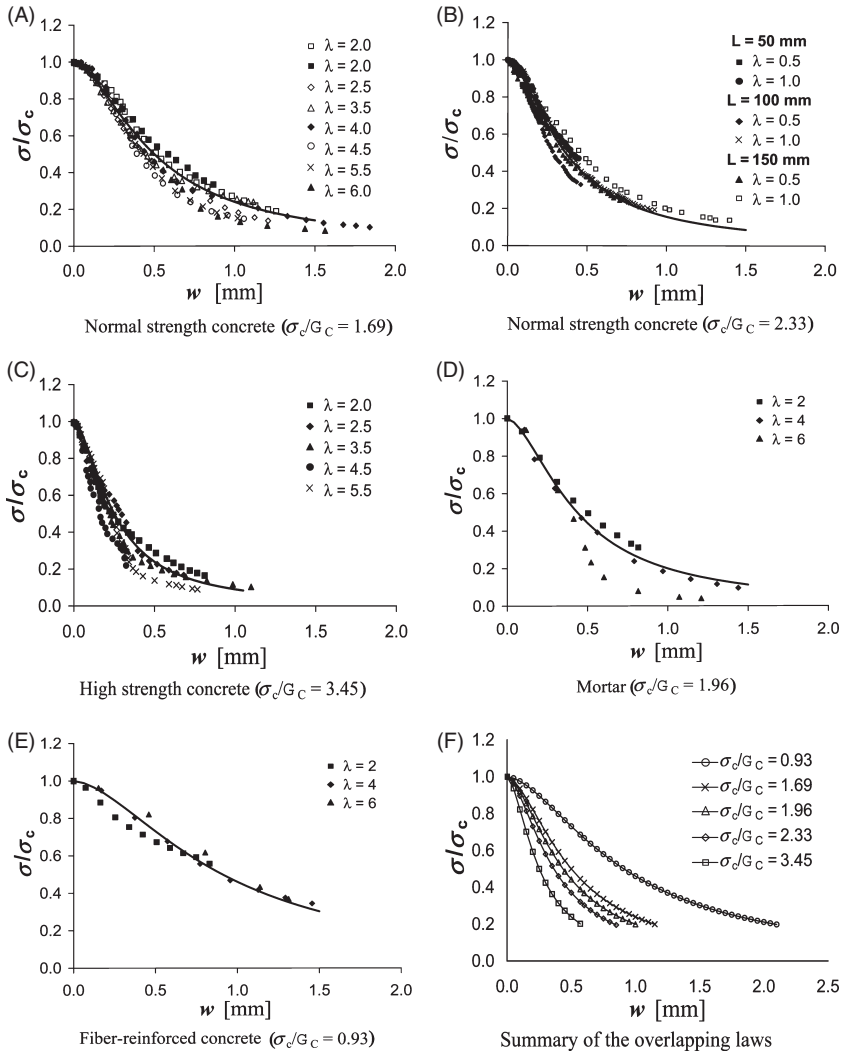

Figure 2: Experimental and best-fitting Overlapping Crack laws for different concrete-like materials. The data in (A) are from [8] (not filled in symbols) and [24] (filled in symbols); those in (B) are from [25]; those in (C) are from [8]; those in (D) are from [24] and those in (E) from [24]. A summary of the best-fitting curves is shown in (F)

Table 1: Mechanical parameters for concrete, mortar and FRC samples tested in [8, 24, 25]

Specimens	E_{ci} (GPa)	E_{cl} (GPa)	σ_c (MPa)	G_C (N mm^{-1})	w_{cr}^c (mm)
NSC [8]	38	28	47.9	28.3	1.15
NSC [24]	35	20	39.9	23.6	1.15
NSC [26]	41	26	42.6	18.3	0.85
HSC [8]	49	40	90.1	26.1	0.57
FRC [24]	36	20	47.7	51.6	2.10
Mortar [24]	38	23	64.9	33.1	1.00

FRC, fibre-reinforced concrete; HSC, high-strength concrete; NSC, normal-strength concrete.

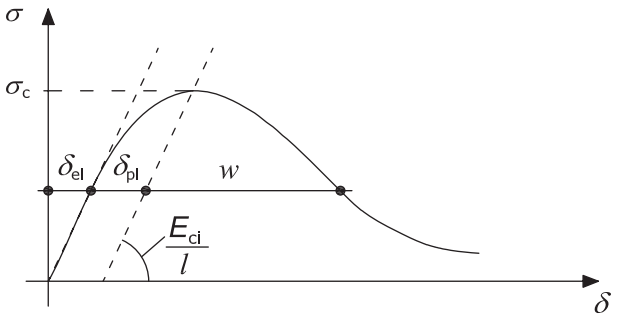

Figure 3: Evaluation of the localised interpenetration, w, from the total shortening of the specimen, δ

value of the ratio $\sigma_c/\mathcal{G}_C$, where the crushing energy has been conventionally computed by numerically integrating the overlapping crack law from $w = 0$ to a critical interpenetration w_{cr} corresponding to $\sigma_r = 0.2\sigma_c$, according to the experimental evidence. It is interesting to note that, whereas the best-fitting parameter B has been set equal to 1.67 for all the considered materials, the remaining free parameter A is linearly dependent on the ratio $\sigma_c/\mathcal{G}_C$ (see Figure 4):

$$A \cong 1.18\sigma_c/\mathcal{G}_C. \tag{4}$$

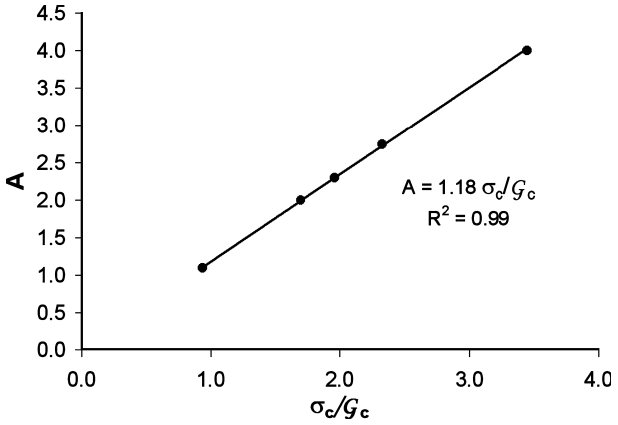

Figure 4: Experimental relationship between the best-fitting parameter A and the brittleness ratio $\sigma_c/\mathcal{G}_C$

Equation (4) suggests that the parameter A is an increasing function of the material brittleness in compression, which is defined, analogously to the brittleness in tension, by the ratio $\sigma_c/\mathcal{G}_C$. The comparison between the constitutive laws obtained for the considered materials highlights that high-strength (HS) concrete (Figure 2C) exhibits the most brittle behaviour, normal-strength (NS) concrete (Figures 2A,B) and mortar (Figure 2D) have an intermediate similar behaviour, and FRC (Figure 2E) has the most ductile behaviour. The introduction of fibres in the mixture, in fact, determines a considerable increment of the crushing energy and of the corresponding critical interpenetration, w_{cr}.

According to the hypotheses of the model previously outlined and using the overlapping crack laws whose parameters are determined according to Equation (4), uniaxial compressive tests can be modelled as shown in Figure 5. In particular, we identify three schematic stages for the application of the model. A first stage where the specimen behaves elastically without any localisation zones and its response is governed by Equation (1) (see Figure 5B). A second stage where, after reaching the ultimate compression strength, σ_c, the deformation starts to localise in a crushing band. The behaviour of this zone is described by the softening law in Equation (2), whereas the outside part of the specimen still behaves elastically (see Figure 5C). The displacement of the upper side can be computed as the sum of the elastic deformation and the interpenetration displacement w:

$$\delta = \varepsilon l + w; \text{for } w \leq w_{cr}, \tag{5}$$

where both ε and w are functions of the stress level, according to, respectively, Equations (1) and (2). While the crushing zone overlaps, the elastic zone expands at progressively decreasing stresses. When $\delta \geq w_c$, concrete in the crushing zone is completely damaged and is able to transfer only a constant residual stress, σ_r (see Figure 5D).

According to this model, very different global responses in the σ–δ diagram can be obtained by varying the mechanical and geometrical parameters of the samples. In particular, the softening process is stable under displacement control, only when the slope $d\sigma/d\delta$ in the unloading regime is negative (Figure 6A). A sudden drop in the load-bearing capacity under displacement control takes place when the slope is infinite (Figure 6B). Finally, a snap-back instability occurs, like that shown in Figure 6C, if the loading process is controlled by means of the localised interpenetration or the lateral strain, when the slope $d\sigma/d\delta$ of the softening branch becomes

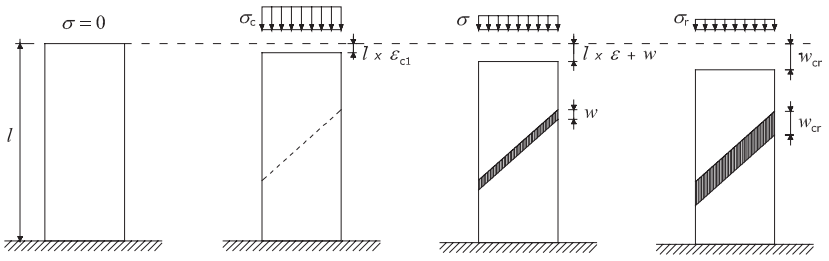

Figure 5: Subsequent stages in the deformation history of a specimen in compression

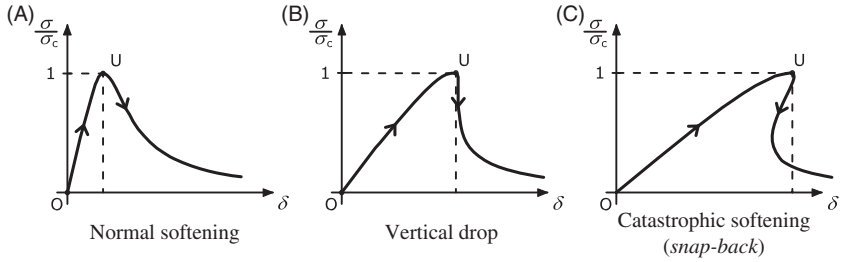

Figure 6: Stress–displacement response

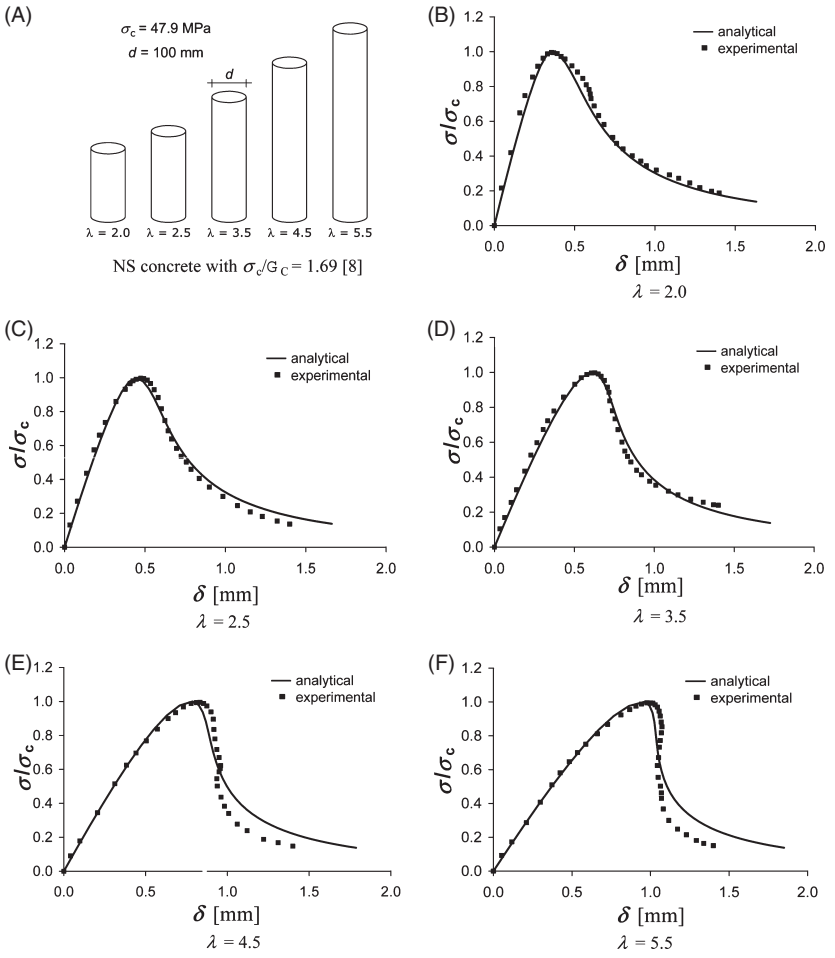

Figure 7: Analytical and experimental stress versus displacement diagrams for normal-strength concrete with $\sigma_c/G_C = 1.69$ and different specimen slendernesses, λ. Experimental data taken from [8]

positive. The proposed model permits to describe such a ductile-to-brittle transition from an analytical point of view. The total shortening of the specimen can be subdivided into three different contributions during the softening regime (see Figure 3):

$$\delta = \delta_{el} + \delta_{pl} + w, \tag{6}$$

where δ_{el} is defined by Equation (3) and δ_{pl} is a constant. The interpenetration w is obtained by rearranging Equation (2) as follows:

$$w = \frac{1}{A}\left(\frac{1}{\tilde{\sigma}} - 1\right)^{\frac{1}{B}}, \tag{7}$$

where $\tilde{\sigma} = \sigma/\sigma_c$, and $1/B = 0.6$.

Normal softening occurs for $d\delta/d\tilde{\sigma} < 0$, i.e. for:

$$\frac{\sigma_c}{E_{ci}} l - \frac{0.6}{A}\left(\frac{\tilde{\sigma}}{1-\tilde{\sigma}}\right)^{0.4}\frac{1}{\tilde{\sigma}} < 0. \tag{8}$$

Such an inequality is satisfied for any values of $\tilde{\sigma}$ if:

$$\frac{\sigma_c}{E_{ci}} lA < 2.72. \tag{9}$$

Introducing in Equation (9) the relationship between A and σ_c/G_C given by Equation (4), we have:

$$1.18\frac{\sigma_c}{E_{ci}} \times \frac{l}{d} \times \frac{\sigma_c d}{\mathcal{G}_C} < 2.72, \tag{10}$$

where d is the specimen width. The ratio $\mathcal{G}_C/(\sigma_c d)$ is dimensionless and is a function of the material properties and of the structural size. Such a parameter is defined as the *energy brittleness number in compression*, s_E^c, and it is analogous to that proposed in [21] for cohesive crack propagation in tension. It describes the scale effects typical of Fracture Mechanics, i.e. the ductile-to-brittle transition when the size-scale increases. Equation (10) can be rewritten in the following form:

$$\frac{s_E^c}{\varepsilon_c^* \lambda} > \frac{1}{2.3}, \tag{11}$$

where $\lambda = l/d$ is the specimen slenderness and ε_c^* is the elastic deformation recovered during the softening unloading.

Hence, catastrophic softening (*snap-back*) occurs for:

$$\frac{s_E^c}{\varepsilon_c^* \lambda} \leq \frac{1}{2.3}. \tag{12}$$

Therefore, when the size-scale and the specimen slenderness are relatively large and the crushing energy relatively low, the global structural behaviour becomes brittle. Moreover, the single values of the parameters s_E^c, ε_c^* and λ are not responsible for the global brittleness or ductility of the structure considered, but only their combination $s_E^c/\varepsilon_c^*\lambda$.

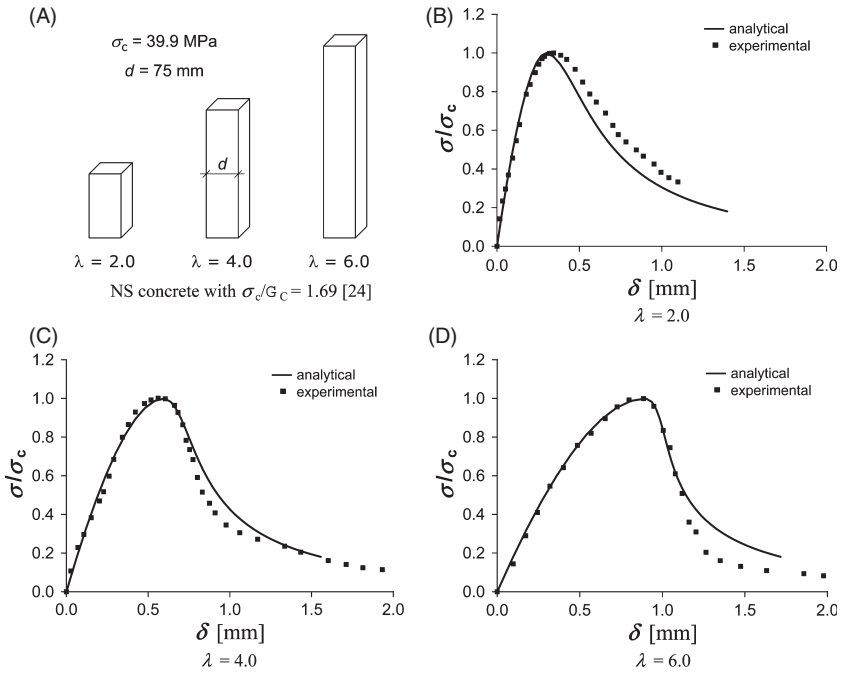

Figure 8: Analytical and experimental stress versus displacement diagrams for normal-strength concrete with $\sigma_c/\mathcal{G}_C = 1.69$ and different specimen slendernesses, λ. Experimental data taken from [24]

Comparison Between Analytical and Experimental Stress–Displacement Curves for Different Materials and Specimen Geometries

In this section, a comparison between the analytical and experimental stress–displacement curves is proposed to show the capabilities of the proposed theoretical model and the accuracy of the overlapping crack constitutive law in Equation (2). Special attention will be given to the effects of the slenderness and of the specimen size. All the experimental data are representative of the behaviour of specimens without lateral confinement, i.e. the samples either have a slenderness higher than 2.0, or have been tested using Teflon.

The effect of the specimen slenderness

Let us consider the experimental programme performed by Jansen and Shah [8] on NS concrete with $\sigma_c = 47.9$ MPa and $\sigma_c/\mathcal{G}_C = 1.69$. They tested cylindrical specimens with $d = 100$ mm and different slenderness $\lambda = 2.0$, 2.5, 3.5, 4.5 and 5.5. A comparison between the experimental stress–displacement data reported with black dots and the analytical predictions in solid line, obtained by setting the parameter A according to Equation (4), is shown in Figure 7. A very good agreement has to be noticed, demonstrating the effectiveness of the proposed approach. Stable softening post-peak branches occur for $\lambda \leq 4.5$, whereas the onset of a snap-back instability is noticed for $\lambda = 5.5$, where the tangent to the stress–displacement curve becomes vertical just after the achievement of the peak load. Another experimental programme on NS concrete with $\sigma_c = 39.9$ MPa and with the same value of $\sigma_c/\mathcal{G}_C = 1.69$ as before was performed by Rokugo and Koyanagi [24] on prismatic specimens with a square base ($d = 75$ mm) and different slendernesses. Here, we consider the data corresponding to $\lambda = 2.0$, 4.0 and 6.0 for a direct comparison with the results by Palmquist and Jansen [14]. Using the same value of the parameter A as for the previous set of experiments, the experimental–analytical comparison is

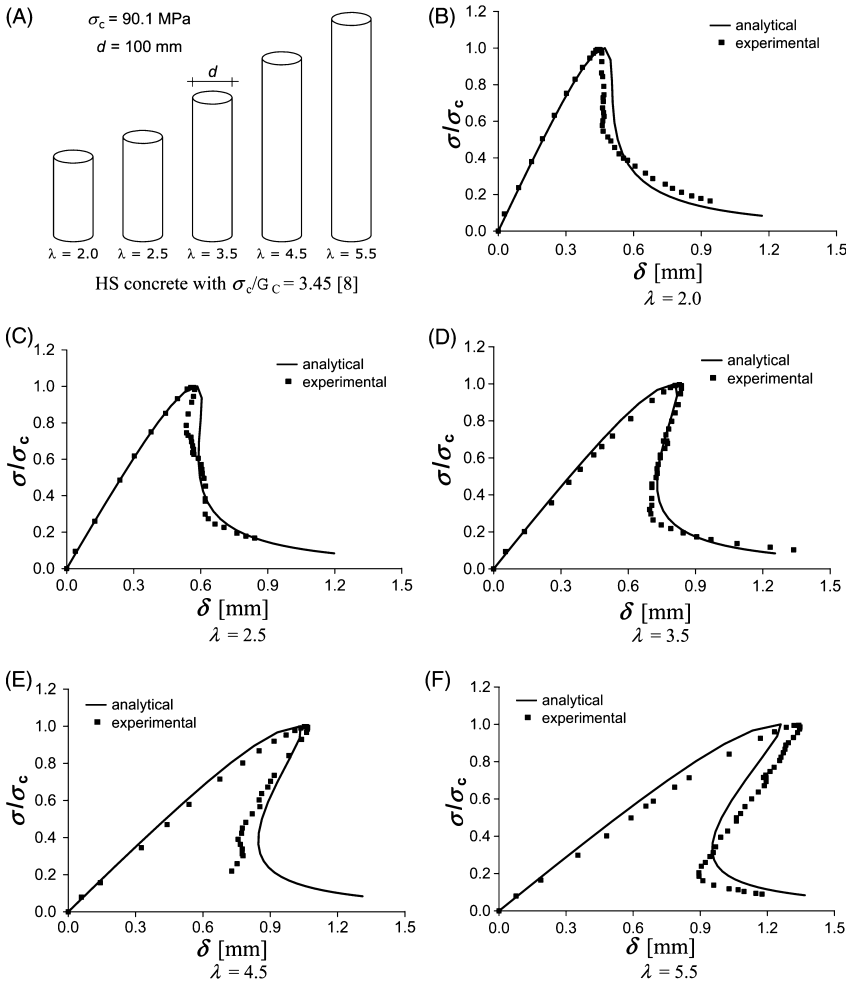

Figure 9: Analytical and experimental stress versus displacement diagrams for high-strength concrete with $\sigma_c/G_C = 3.45$ and different specimen slendernesses, λ. Experimental data taken from [8]

shown in Figure 8. Again, a very good agreement between the model predictions and the experimental results is evidenced.

As far as HS concrete is concerned, Jansen and Shah [8] tested cylindrical samples with $\sigma_c = 90.1$ MPa, $\sigma_c/\mathcal{G}_C = 3.45$, $d = 100$ mm and different slendernesses $\lambda = 2.0$, 2.5, 3.5, 4.5 and 5.5. A comparison between the experimental stress–displacement data reported with black dots and the analytical predictions in solid line is shown in Figure 9. In this case, the slope of the stress–displacement relationship of the post-peak branch becomes positive for $\lambda \geq 2.5$, giving rise to severe snap-back instabilities. The proposed model with the parameter A computed as a function of $\sigma_c/\mathcal{G}_C$ according to Equation (4) is able to predict closely the experimental response, capturing the transition from stable softening to snap-back branches by increasing the specimen slenderness. Similar mechanical instabilities because of size-scale effects and softening behaviour have also been evidenced in granular materials, such as sand, subjected to multiaxial compression. In this case, the post-peak analysis is carried out by assuming a strain localisation induced by the development of shear bands, as proposed in the model by Gajo *et al.* [26], although with a completely different approach from that herein introduced.

Finally, to prove the predictive capabilities of the proposed model also for other materials, we consider the experimental data by Rokugo and Koyanagi [24] on mortar ($\sigma_c = 64.9$ MPa, $\sigma_c/\mathcal{G}_C = 1.96$) and on FRC ($\sigma_c = 47.7$ MPa, $\sigma_c/\mathcal{G}_C = 0.93$). They tested prismatic specimens with a square base ($d = 75$ mm) and $\lambda = 2.0$, 4.0 and 6.0 (see also Palmquist and Jansen [14]). The analytical–experimental comparisons for the two materials are shown, respectively, in Figures 10 and 11. Also in this case, the proposed model is able to predict the slenderness dependence of the experimental stress–displacement curves by setting the value of the parameter A according to Equation (4) for the two materials.

The effect of the specimen size

The mechanical response of uniaxial compression tests is not only a function of the specimen slenderness, but also of the specimen size, as experimentally shown by Ferrara and Gobbi [25]. In particular, they considered prismatic specimens made of NS concrete with $\sigma_c = 42.6$ MPa, $\sigma_c/\mathcal{G}_C = 2.33$, three different size-scales and two different values of the slenderness, $\lambda = 0.5$ and 1.0. Note that none of these cases can be modelled according to the approach proposed by Palmquist and Jansen [14], which is strictly limited to specimens with $\lambda \geq 2$. The analytical–experimental comparison for the data sets with $\lambda = 0.5$ and 1.0 is proposed, respectively, in Figures 12 and 13. Also in this case, a very good agreement between the theoretical and the experimental curves is achieved.

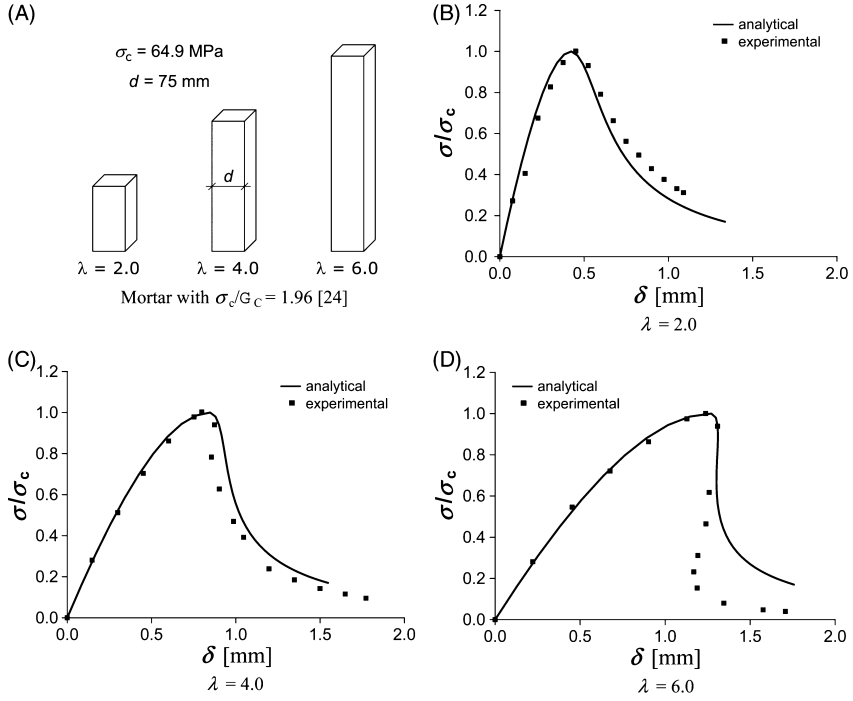

Figure 10: Analytical and experimental stress versus displacement diagrams for mortar with $\sigma_c/\mathcal{G}_C = 1.96$ and different specimen slendernesses, λ. Experimental data taken from [24]

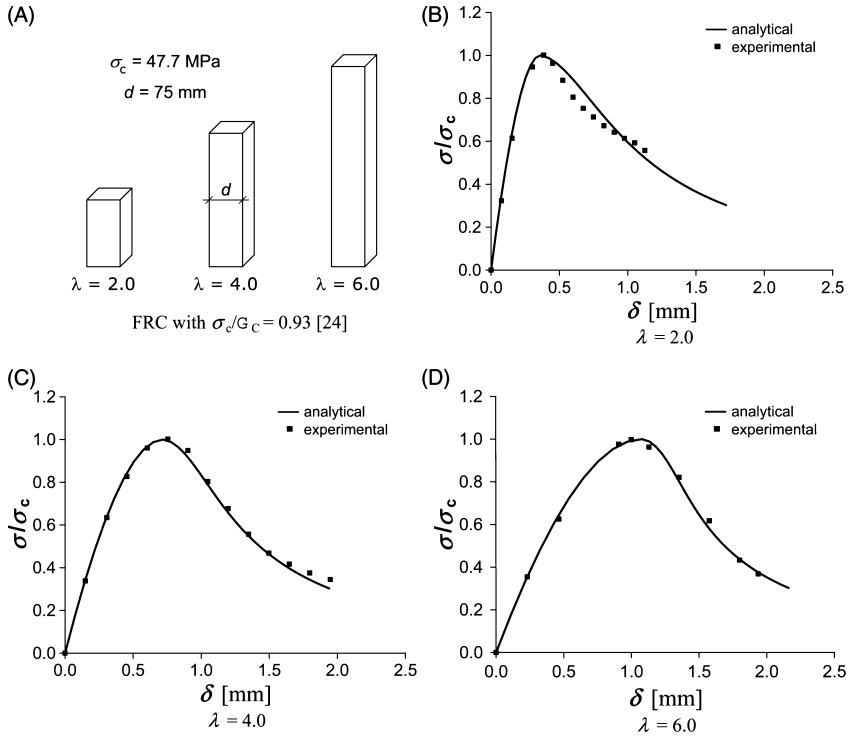

Figure 11: Analytical and experimental stress versus displacement diagrams for fibre-reinforced concrete with $\sigma_c/\mathcal{G}_C$ = 0.93 and different specimen slendernesses, λ. Experimental data taken from [24]

Conclusions

In this paper, we have proposed an analytical model for the study of uniaxial compression tests based on the evidence that the post-peak dissipated energy referred to a unitary surface can be considered as a material property and that the post-peak stress–displacement relationship is independent of the specimen size. This new approach, referred to as *Overlapping Crack Model*, is suitable for the analysis of quasi-brittle materials in compression, regardless of the actual failure mode of the tested

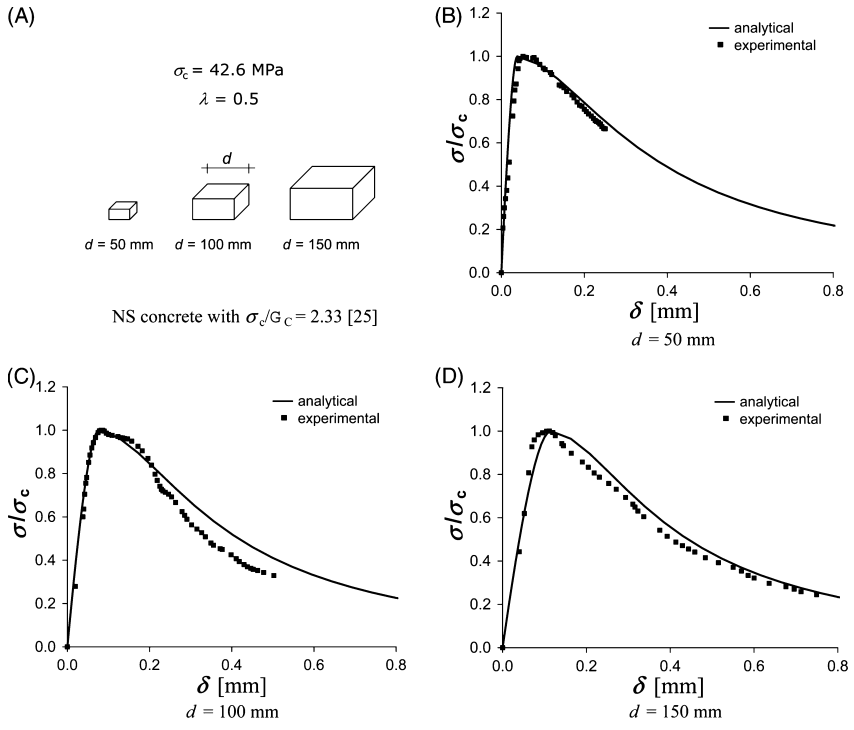

Figure 12: Analytical and experimental stress versus displacement diagrams for normal-strength concrete with $\sigma_c/\mathcal{G}_C$ = 2.33, different specimen sizes and λ = 0.5. Experimental data taken from [25]

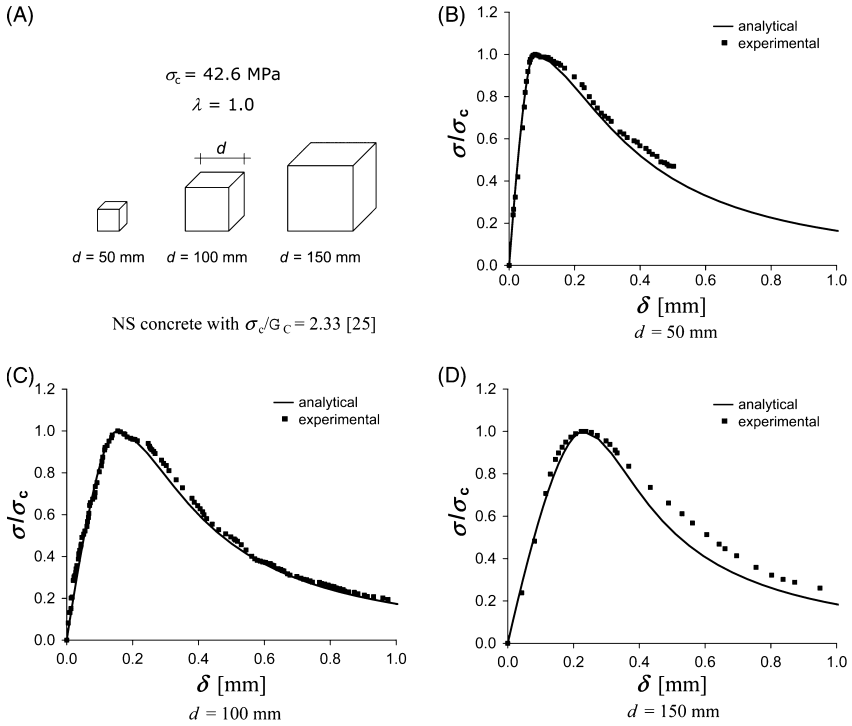

Figure 13: Analytical and experimental stress versus displacement diagrams for normal-strength concrete with $\sigma_c/\mathcal{G}_C$ = 2.33, different specimen sizes and λ = 1.0. Experimental data taken from [25]

specimen. In fact, an examination of experimental results shows that the structural collapse may range from diagonal shear crack propagation to splitting, or even to pure concrete crushing, depending on the slenderness and the size-scale of the unconfined sample. The micromechanical model by Nemat-Nasser and Horii [27] and the computational approach by Carpinteri *et al.* [28] can be used to describe the growth of a population of tensile cracks and the formation of shear bands and crack patterns typical of diagonal shear failure or concrete splitting. However, when the slenderness decreases, a transition from splitting to crushing collapse occurs and these micromechanics approaches should leave place to fragmentation-based models. Hence, the fictitious concept of overlapping crack, analogous to the cohesive crack in tension, permits to avoid the elaborate description of the kinematics of each failure mode, which depends on the specimen geometry.

It has been shown how to determine the stress–interpenetration relationship from experimental data and that this has the advantage of being characterised by a single free parameter that can be related to the ratio between the compression strength and the crushing energy (see Figure 4). The wide comparison between the analytical and experimental stress–displacement curves for mortar, plain concrete and FRC has shown the effectiveness and accuracy of the present approach to capture both stable softening or sharp snap-back post-peak branches by varying the slenderness or the size-scale of the tested samples.

ACKNOWLEDGEMENT

The financial support of the European Union to the Leonardo da Vinci Project I/06/B/F/PP-154069 'Innovative Learning and Training On Fracture' (ILTOF) is gratefully acknowledged.

REFERENCES

1. Kotsovos, M. D. (1983) Effect of testing technique on the post-ultimate behaviour of concrete in compression. *Mater. Struct.* **16**, 3–12.
2. van Mier, J. G. M. (1984) *Strain Softening of Concrete Under Multiaxial Compression*. PhD Thesis, Eindhoven University of Technology, The Netherlands.
3. van Mier, J. G. M., Shah, S. P., Arnaud, M., *et al.* (1997) Strain-softening of concrete in uniaxial compression. *Mater. Struct.* **30**, 195–209.
4. Indelicato, F. and Paggi, M. (2008) Specimen shape and the problem of contact in the assessment of concrete compressive strength. *Mater. Struct.* **41**, 431–441.
5. Carpinteri, A., Ciola, F., Pugno, N., Ferrara, G. and Gobbi, E. (2001) Size-scale and slenderness influence on the compressive strain-softening behaviour of concrete. *Fatigue Fract. Eng. Mater. Struct.* **24**, 441–450.
6. Dahl, H. and Brincker, R. (1989) Fracture energy of high-strength concrete in compression. In: *Fracture of Concrete and Rock – Recent Developments* (S. P. Shah, B. Barr and S. E. Swartz, Eds) (Proc. Int. Conf. on Recent Developments in the Fracture of Concrete and Rock, Cardiff, Wales, 1989). Elsevier Applied Science, England: 523–536.

7. van Vliet, M. and van Mier, J. (1996) Experimental investigation of concrete fracture under uniaxial compression. *Mech. Cohesive-Frictional Mater.* **1**, 115–127.
8. Jansen, D. C. and Shah, S. P. (1997) Effect of length on compressive strain softening of concrete. *J. Eng. Mech.* **123**, 25–35.
9. Suzuki, M., Akiyama, M., Matsuzaki, H. and Dang, T. H. (2006) Concentric loading test of RC columns with normal- and high-strength materials and averaged stress-strain model for confined concrete considering compressive fracture energy. *Proc. 2nd fib Congress*. Naples, Italy, CD-ROM, ID 3-13.
10. Hudson, J. A., Brown, E. T. and Fairhurst, C. (1972) Shape of the complete stress-strain curve for rock. *Proc. 13th Symposium on Rock Mechanics*, University of Illinois, Urbana, IL, 1971, American Society of Civil Engineers, 773–795.
11. Hillerborg, A. (1990) Fracture mechanics concepts applied to moment capacity and rotational capacity of reinforced concrete beams. *Eng. Fract. Mech.* **35**, 233–240.
12. Markeset, G. and Hillerborg, A. (1995) Softening of concrete in compression - localization and size effects. *Cem. Concr. Res.* **25**, 702–708.
13. Bažant, Z. P. (1989) Identification of strain-softening constitutive relation from uniaxial tests by series coupling model for localization. *Cem. Concr. Res.* **19**, 973–977.
14. Palmquist, S. M. and Jansen, D. C. (2001) Postpeak strain–stress relationship for concrete in compression. *ACI Mater. J.* **98**, 213–219.
15. Carpinteri, A., Corrado, M., Paggi, M. and Mancini, G. (2007) Cohesive versus overlapping crack model for a size effect analysis of RC elements in bending. In: *Design, Assessment and Retrofitting of RC Structures, Vol. 2 of the Proceedings of the 6th Conference on Fracture Mechanics of Concrete and Concrete Structures (FraMCoS)* (A. Carpinteri, P. Gambarova, G. Ferro and G. Plizzari, Eds). Taylor & Francis, Catania, Italy: 655–663.
16. Carpinteri, A., Corrado, M., Paggi, M. and Mancini, G. (2009) New model for the analysis of size-scale effects on the ductility of reinforced concrete elements in bending. *ASCE J. Eng. Mech* **135**, 221–229.
17. Carpinteri, A., Corrado, M., Mancini, G. and Paggi, M. (2009) A numerical approach to modelling size effects on the flexural ductility of RC beams. *Mater. Struct.* **42**, 1353–1367. doi: 10.1617/s11527-008-9454-y
18. Corrado, M. (2007) *Effetti di Scala sulla Capacità di Rotazione Plastica di Travi in Calcestruzzo Armato*. PhD Thesis, Politecnico di Torino, Torino, Italy (in Italian).
19. Hillerborg, A., Modeer, M. and Petersson, P. E. (1976) Analysis of crack formation and crack growth in concrete by means of fracture mechanics and finite elements. *Cem. Concr. Res.* **6**, 773–782.
20. Petersson, P. E. (1981) *Crack Growth and Development of Fracture Zones in Plain Concrete and Similar Materials*. Technical Report, LUTVDG/TVBM-1006, Lund Institute of Technology, Lund, Sweden.
21. Carpinteri, A. (1985) Interpretation of the Griffith instability as a bifurcation of the global equilibrium. In: *Application of Fracture Mechanics to Cementitious Composites* (S. P. Shah, Ed.) (Proc. NATO Advanced Research Workshop, Evanston, USA, 1984). Martinus Nijhoff Publishers, Dordrecht: 287–316.
22. Carpinteri, A. (1989) Cusp catastrophe interpretation of fracture instability. *J. Mech. Phys. Solids* **32**, 567–582.
23. Comité Euro-International du Béton (1993) *CEB-FIP Model Code 1990*. Thomas Telford Ltd, Lausanne, CEB Bulletin No. 213/214.
24. Rokugo, K. and Koyanagi, W. (1992) Role of compressive fracture energy of concrete on the failure behaviour of reinforced concrete beams. In: *Applications of Fracture Mechanics to Reinforced Concrete* (A. Carpinteri, Ed.). Elsevier Applied Science, London: 437–464.
25. Ferrara, G. and Gobbi, M. E. (1995) *Strain Softening of Concrete Under Compression*. Report to RILEM Committee 148-SSC, ENEL-CRIS Laboratory, Milano, Italy.
26. Gajo, A., Bigoni, D. and Muir Wood, D. (2004) Multiple shear band development and related instabilities in granular materials. *J. Mech. Phys. Solids* **52**, 2683–2724.
27. Nemat-Nasser, S. and Horii, H. (1984) Rock failure in compression. *Int. J. Eng. Sci.* **22**, 999–1011.
28. Carpinteri, A., Ciola, F. and Pugno, N. (2001) Boundary element method for the strain-softening response of quasi-brittle materials in compression. *Comput. Struct.* **79**, 389–401.

